MRS Communications (2018), *8*, 1244–1253
© Materials Research Society, 2018
doi:10.1557/mrc.2018.119

MRS Communications

Research Letter

Perovskite solar cells based on hole-transporting conjugated polymers by direct arylation polycondensation

Wei Li, Takehiko Mori, and **Tsuyoshi Michinobu,** Department of Materials Science and Engineering, Tokyo Institute of Technology, 2-12-1 Ookayama, Meguro-ku, Tokyo 152-8552, Japan

Address all correspondence to Tsuyoshi Michinobu at **michinobu.t.aa@m.titech.ac.jp**

(Received 12 May 2018; accepted 22 June 2018)

Abstract

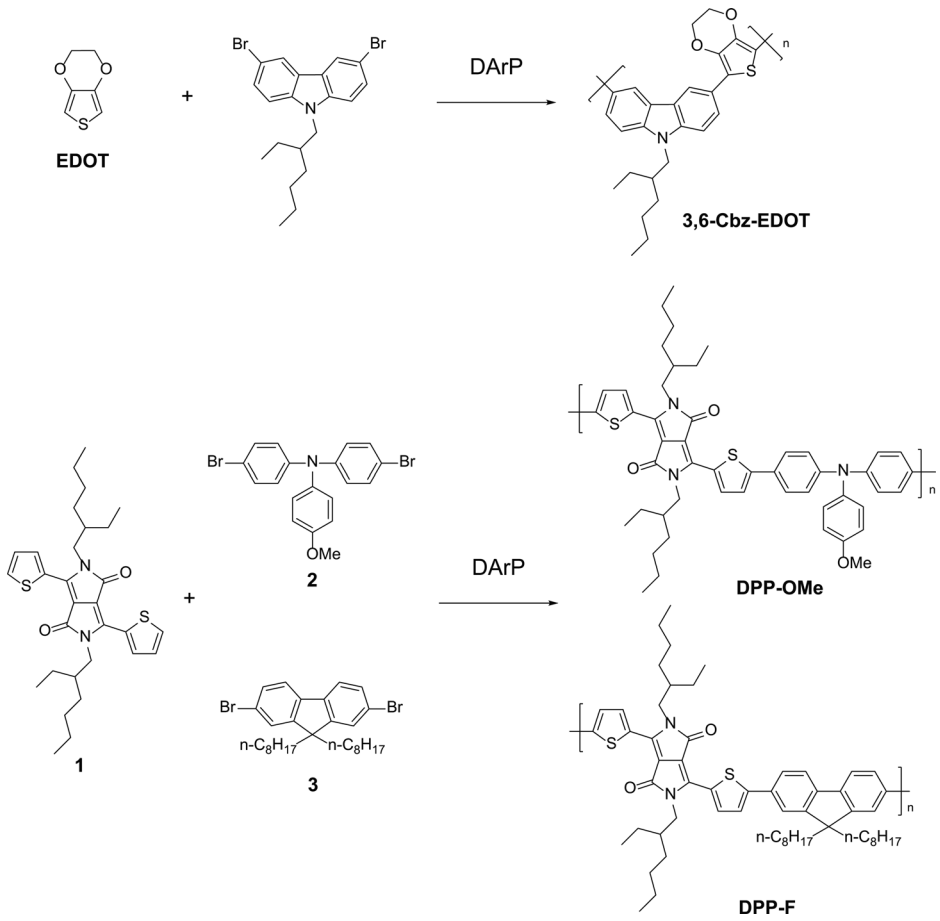
Direct arylation polycondensation (DArP) is an emerging synthetic method of producing conjugated polymers in an environmentally benign and cost-effective manner. We now report the synthesis of hole-transporting conjugated polymers, namely, **DPP-OMe** (M_n = 7.9 kg/mol) and **DPP-F** (M_n = 12.6 kg/mol), under microwave-assisted DArP conditions. These two polymers and the previously synthesized **3,6-Cbz-EDOT** were evaluated as hole-transporting materials in mesoscopic perovskite solar cells. **3,6-Cbz-EDOT** synthesized by DArP exhibited higher hole mobility and better photovoltaic properties than that synthesized by the Stille polycondensation. Moreover, chemical dopants improved the short-circuit current density (J_{sc}) and fill factor.

Introduction

Hole-transporting conjugated polymers have been an important component in many high-performance thin film devices, such as perovskite solar cells (PSCs) and organic light-emitting diodes (OLEDs).[1–7] Aromatic amine compounds are good examples and they could improve the device performances when they carry holes within the multilayer devices. For example, 2,2,7,7-tetrakis(*N*,*N*-di-*p*-methoxyphenylamine)-9,9-spirobifluorene (spiro-OMeTAD) has been a benchmark hole-transporting material (HTM) in PSCs,[8] and this was also the case for *N*,*N*′-diphenyl-*N*,*N*′-bis(3-methylphenyl)-1,1′-diphenyl-4,4′-diamine and tris (4-carbazoyl-9-ylphenyl)amine in OLEDs.[9] Based on these benchmark compounds, a series of aromatic polyamines, such as poly[bis(4-phenyl)(2,4,6-trimethylphenyl)amine],[10] were also developed and their thin films were fabricated by wet processes in the multilayer devices.[11–22] Recently, narrow bandgap *p*-type semiconducting polymers appeared as high mobility organic materials, which were mainly used in thin film transistors (TFTs) and bulk-heterojunction polymer solar cells.[23–27] These polymers are composed of alternating donor and acceptor structures, and their narrow bandgaps originate from the intramolecular charge–transfer (CT) interactions. For example, 3,6-dithiophen-2-yl-2,5-dihydropyrrole[3,4-*c*]pyrrole-1,4-dione (DTDPP) is one of the most often used CT chromophores to design high-performance narrow bandgap polymers.[28–30] Due to the lactam structure, they show strong π–π interactions, forming highly crystalline films with high mobilities.

Both aromatic polyamines and narrow bandgap *p*-type polymers have been synthesized by the Pd-catalyzed polycondensation, such as the Suzuki and Stille polycondensations. However, these conventional polycondensations required the multistep tedious preparation of bifunctional boronic acids (for Suzuki coupling) and tin compounds (for Stille coupling), and a stoichiometric amount of toxic byproducts was produced by the polycondensations. In this century, in order to establish environmentally benign and cost-effective syntheses of these polymers, direct arylation polycondensatoin (DArP) was introduced.[31–39] This polycondensation utilizes the C–H bond activation of unprepared arenes and heteroarenes, and accordingly, the reaction step of the monomer synthesis can be shortened.[40–45] Also, since trialkyltin functional groups (for Stille coupling) are unnecessary, no toxic byproducts are formed. The byproducts are not desired because they are toxic and become impurities that degrade the device performances. Kanbara and coworkers reported a seminal work that *p*-type semiconducting polymers synthesized by DArP show better photovoltaic performances in bulk-heterojunction solar cells than those synthesized by the conventional Pd-catalyzed polycondensation.[46] Our group recently succeeded in producing one of the promising aromatic polyamines or *p*-type semiconducting polymers, namely, the carbazole-based polymer, **3,6-Cbz-EDOT** (Scheme 1), by microwave-assisted DArP.[47] However, its photovoltaic property of this DArP polymer has not been studied in any type of device.[48] Therefore, we became interested in the application of this polymer as the hole-transporting layer of the PSCs. At the same time, we decided to compare the photovoltaic properties with those of **3,6-Cbz-EDOT** synthesized by the Stille polycondensation. Moreover, during the course of this study, we synthesized DTDPP-based polymers by DArP and investigated

https://doi.org/10.1557/mrc.2018.119 Published online by Cambridge University Press



Scheme 1. Synthesis of hole-transporting polymers by direct arylation polycondensation (DArP).

them as HTMs of PSCs, since the high mobility polymers were relatively unexplored in this field. It was shown that the photovoltaic performances were improved by adding dopants to the hole-transporting layers.

Experimental section

Materials

All the commercially available solvents and reagents were used without further purification unless stated otherwise.

Measurements

^{1}H NMR and ^{13}C NMR spectra were measured on a JEOL model AL300 spectrometer at 20 °C. Chemical shifts are reported in ppm downfield from $SiMe_4$, using the solvent's residual signal as an internal reference. Fourier transform infrared spectra were recorded on a JASCO FT/IR-4100 spectrometer in the range from 4000 to 600/cm. Gel permeation chromatography (GPC) was measured on a JASCO GULLIVER 1500 equipped with a pump (PU-2019 Plus), an absorbance detector (RI-2031 Plus), and two Shodex GPC KF-803 columns (8.0 mm I.D. × 300 mm/L) based on a conventional calibration curve using polystyrene standards. 1,2-Dichlorobenzene (*o*DCB) was used as a carrier solvent at the flow rate of 1.0 mL/min. Thermogravimetric analysis (TGA) and differential scanning calorimetry (DSC) were carried out on a Rigaku Thermoplus TG8120 and DSC8230, respectively, under flowing nitrogen at the scan rate of 10 °C/min. UV-vis absorption spectra were measured on a JASCO V-670 spectrophotometer. Electrochemistry measurements were carried out on a BAS electrochemical analyzer model 612C at 25 °C in dehydrated CH_3CN containing 0.1 M $(n\text{-}C_4H_9)_4NPF_6$ in the three electrode cell. The working, reference, and auxiliary electrodes were a glassy carbon electrode, $Ag/Ag^+/CH_3CN/(n\text{-}C_4H_9)_4NPF_6$, and a Pt wire, respectively. Scanning electron microscopy (SEM) measurements were carried out on a Hitachi S-4700 instrument at the accelerating voltage of 50 kV. Contact angles were measured by a Phoenix 150S analyzer by adding a water drop on the thin film surfaces.

Top-contact/bottom-gate field-effect transistor (FET) devices were fabricated using an n^+-Si/SiO_2 substrate where n^+-Si and SiO_2 were used as the gate electrode and gate dielectric, respectively. The substrate was washed by acetone, 2-propanol, and deionized water under microwave irradiation. The substrate was further cleaned by a Model 208 UV-O_3 cleaning

https://doi.org/10.1557/mrc.2018.119 Published online by Cambridge University Press

system. The cleaned substrate was modified by octadecyltrichlorosilane to form a self-assembled monolayer. The polymer solutions in CH_2Cl_2 (5.0 g/mL) were spin-coated on the surface of treated substrates to form the polymer thin film (40–60 nm thickness) in the air. After that, 50 nm thick gold was deposited as the source and drain contacts using a shadow mask. The TFT devices had a channel length (L) of 100 μm and a channel width (W) of 1 mm. The FET performances were measured in the air using a Keithley 4200 parameter analyzer on a probe stage. The hole mobility, μ, was calculated from the data in the saturated regime using the following equation:

$$I_{SD} = (L/2W)C_i\mu(V_G - V_T)^2, \quad (1)$$

where I_{SD} is the drain current in the saturated regime, W and L are the semiconductor channel width and length, respectively, C_i ($C_i = 13.7$ nF/cm^2) is the capacitance per unit area of the gate dielectric layer, and V_G and V_T are the gate voltage and threshold voltage, respectively. $V_G - V_T$ of the devices was determined from the square root values of I_{SD} at the saturated regime.

A hole-only device was fabricated by using an ITO glass substrate. The device structure was ITO/PEDOT:PSS/HTM/Au. The active area was 0.04/cm^2. First, the ITO glass was etched and cleaned. Then, an isopropanol-treated PEDOT:PSS solution was spin-coated at 4000 rpm for 45 s. This was followed by the formation of HTM layers by spin-coating a chlorobenzene solution (10 mg/mL) at 2000 rpm for 30 s in the air. Finally, gold was vacuum evaporated on the top of the HTMs as metal contact with the thickness of 80 nm. Hole mobilities of HTMs were measured by a space-charge-limited current (SCLC) method. The data in the SCLC regime were fitted using the Mott–Gurney law[24]:

$$J = 9me_0e_rV^2/8d^3, \quad (2)$$

where J is the current density, V is the applied voltage, and d is the thickness of HTM films. The vacuum dielectric constant (ε_0) was considered to be 8.854×10^{-12} C/V/m. The relative dielectric constant (ε_r) was chosen to be 3, and the built-in potential between PEDOT:PSS and Au to be zero.

Synthesis

Synthesis of 2,5-bis(2-ethylhexyl)-3,6-di(thiophen-2-yl)pyrrolo[3,4-*c*]pyrrole-1,4-dione (**1**): In an oven-dried two-necked 100 mL round-bottom flask, a mixture of 3,6-dithiophen-2-yl-2,5-dihydropyrrolo[3,4-*c*]pyrrole-1,4-dione (1.00 g, 3.30 mmol) and anhydrous K_2CO_3 (1.52 g, 11.0 mmol) were dissolved in anhydrous *N*,*N*-dimethylformamide (DMF, 24 mL) and heated to 120 °C under N_2 for 1 h. 1-Bromo-2-ethylhexane (1.96 g, 10.0 mmol) was then added dropwise, followed by the addition of a small amount of 18-crown-6. The reaction mixture was further stirred at 150 °C overnight before being cooled to room temperature and poured into distilled water (200 mL). After stirring the resulting suspension at room temperature for 1 h, the solid was collected by vacuum filtration, washed with several portions of distilled water and methanol, and then dried under vacuum. The crude product was purified by column chromatography (SiO_2, hexane/EtOAc 4:1) to yield a dark red solid (0.60 g, 70%). ^{1}H NMR (300 MHz, $CDCl_3$) δ 8.90 (dd, $J = 3.8$, 1.0 Hz, 2H), 7.64 (dd, $J = 4.9$, 1.1 Hz, 2H), 7.27 (d, $J = 2.6$ Hz, 2H), 4.03 (dd, $J = 7.6$, 3.5 Hz, 4H), 1.61 (s, 2H), 1.29 (dd, $J = 21.5$, 5.8 Hz, 16H), 0.86 ppm (s, 12H). ^{13}C NMR (75 MHz, $CDCl_3$) δ 162.50, 141.14, 135.99, 131.23, 130.50, 129.11, 108.56, 46.40, 39.60, 30.71, 28.87, 24.03, 23.58, 14.53, 10.97 ppm. IR (neat): $\nu = 2956$, 2928, 2858, 2223, 1726, 1674, 1568, 1486, 1452, 1404, 1319, 1291, 1269, 1232, 1099, 1070, 852, 823, 718, 669, 609/cm.

Synthesis of 4-methoxy-*N*,*N*-bis(4-bromophenyl)aniline (**2**): A solution of *N*-bromosuccinimide (0.72 g, 4.00 mmol) in DMF (10 mL) was added dropwise under stirring to a solution of 4-methoxytriphenylamine (0.55 g, 2.00 mmol) in DMF (10 mL) at 0 °C. The resulting solution was allowed to stir at room temperature overnight. Water was added to quench the reaction. Then, the organic layer was extracted by dichloromethane, the solvent was evaporated. Recrystallization from hexane yielded the desired product (0.60 g, 75%). ^{1}H NMR (300 MHz, $CDCl_3$) δ 7.41–7.30 (m, 4H), 7.06 (d, $J = 8.9$ Hz, 2H), 6.98–6.81 (m, 6H), 3.83 ppm (s, 3H). ^{13}C NMR (75 MHz, $CDCl_3$) δ 156.73, 146.81, 139.70, 132.16, 127.40, 124.24, 114.98, 114.49, 55.38 ppm. IR (neat): $\nu = 1579$, 1506, 1484, 1313, 1282, 1241, 1177, 1104, 1072, 1035, 1007, 907, 862, 821, 787, 735, 704, 682, 665, 649, 634, 622/cm.

DArP procedure: Dibromo-monomer (0.2 mmol) and compound **1** or EDOT (0.2 mmol) were added to a reaction tube. The tube was transferred to a glove box under argon atmosphere. Then, 5.0 mol.% of $Pd(OAc)_2$, 1.5 equiv. of potassium pivalate (PivOK), and DMAc (2.0 mL) were added. The tube was sealed, removed from the glove box, and heated to 120 °C for 1 h under microwave irradiation. The reaction mixture was cooled to room temperature, and the residue was washed by water, methanol, and hexane. The soluble polymers were collected by using a Soxhlet extractor using dichloromethane. The extracted solutions were concentrated and reprecipitated into hexane, yielding the desired polymers. For the characterization data of **3,6-Cbz-EDOT**, see Refs. 47 and 48.

DPP-OMe: ^{1}H NMR (300 MHz, $CDCl_3$) δ 9.00 (br, Ar-H), 7.56 (br, Ar-H), 7.37 (br, Ar-H), 7.32–6.32 (br, Ar-H), 6.92 (d br, Ar-H), 4.07 (br, CH_2), 3.90 (br, CH_3), 1.57 (br, CH), 1.51–0.78 (br, CH_2), 0.78–0.49 ppm (br, CH_3). IR (neat): $\nu = 2929$, 2377, 2321, 1663, 1556, 1506, 1433, 1320, 1276, 751, 718, 636, 608/cm. GPC (oDCB): $M_n = 7.9$ kg/mol, $M_w/M_n = 2.2$. Yield 62%.

DPP-F: ^{1}H NMR (300 MHz, $CDCl_3$) δ 9.04 (br, Ar-H), 7.85–7.62 (br, Ar-H), 7.58 (br, Ar-H), 4.14 (br, CH_2), 1.61 (br, CH), 1.44–1.01 (br, CH_2), 0.95 (br, CH_2), 0.80 ppm (br, CH_3). IR (neat): $\nu = 2927$, 2371, 2350, 2315, 1738, 1668, 1542, 1509, 1457, 1421, 1373, 1239, 1079, 1025, 732, 687, 638, 609/cm. GPC (oDCB): $M_n = 12.6$ kg/mol, $M_w/M_n = 2.6$. Yield 57%.

https://doi.org/10.1557/mrc.2018.119 Published online by Cambridge University Press

Fabrication and measurements of PSCs

Fluorine-doped tin oxide (FTO)-coated glass substrates (Tec 7, Pilkington) were patterned to fabricate the solar cells. These substrates were successively washed by ultrasonication in water, acetone, and isopropanol for 20 min each, and then dried in a stream of dry air. The washed substrates were further treated with a UV-O_3 cleaner (Filgen, Model UV253E) for 30 min. The electron-accepting TiO_2 compact layer was spin-coated (1500 rpm for 30 s) from 0.2 M titanium(IV) isopropoxide bis(acetylacetonate) in anhydrous ethanol (70 µL) and sintered at 100 °C for 5 min, and then annealed at 500 °C for 30 min. After cooling to room temperature, the obtained films were immersed into 20 mM $TiCl_4$ solution at 70 °C for 30 min. After cleaning with deionized water and ethanol, the films were sintered at 500 °C for 30 min. The mesoporous TiO_2 layer composed of 20 nm-sized particles was deposited by spin-coating at 3000 rpm for 60 s using a commercial TiO_2 paste (PST-18NR, JGC Catalysts and Chemicals Ltd., Japan) diluted in ethanol (100 µL, 2:7 wt/wt). After drying at 160 °C for 5 min, the TiO_2 films were gradually heated to 500 °C and baked at this temperature for 30 min. After cooling to room temperature, the obtained films were immersed into 20 mM $TiCl_4$ solution at 70 °C for 30 min, and cleaned with deionized water and ethanol again. The films were sintered at 500 °C for 30 min once time. After this, all the processes were done in an Ar-filled glove box. The mesoporous TiO_2 films were infiltrated with PbI_2 by spin-coating a PbI_2 solution in DMF (465 g/L) at 70 °C. After both PbI_2 solution and devices were heated to 70 °C for 1 h, PbI_2 solution (70 µL) was spin-coated at 4000 rpm for 30 s. After heating to 100 °C for 10 min, the devices were cooled down to room temperature, and a CH_3NH_3I solution (160 µL, 10 mg/mL in isopropanol) was dropped onto the as-prepared PbI_2 film with a loading time of 20 s, followed by spin-coating at 4500 rpm for 20 s. Afterward, the films were annealed at 100 °C for 10 min on a hot plate. After cooling down to the room temperature, a HTM solution (70 µL) was dropped onto the $CH_3NH_3PbI_3$-coated substrates and spin-coated at 500 rpm for 5 s followed by 3000 rpm for 30 s. Four different HTM solutions were employed as follows:

(1) Pristine solution: polymer (10 mg) dissolved in chlorobenzene (1 mL);
(2) The bis(trifluoromethane)sulfonimide lithium salt (Li-TFSi) solution: polymer (10 mg) dissolved in chlorobenzene (1 mL) with Li-TFSi solution (20 µL, 28.3 mg/mL in acetonitrile);
(3) The *tert*-butyl pyridine (TBP) solution: polymer (10 mg) dissolved in chlorobenzene (1 mL) with TBP (10 µL);
(4) Li-TFSi and TBP solution: polymer (10 mg) dissolved in chlorobenzene (1 mL) with Li-TFSi solution (20 µL, 28.3 mg/mL in acetonitrile) and TBP (10 µL).

Finally, 80 nm of Au electrode was thermally evaporated onto the HTM layer using a shadow mask to pattern the electrode.

The current density–voltage (J–V) characteristics and incident photon current efficiency (IPCE) of the fabricated PSCs were evaluated. The active area of the devices was 0.25 cm^2. The J–V curves were measured on a solar simulated (Peccell PEC-L11) under illumination of a solar simulator with a light intensity of 100 mW/cm^2 (AM 1.5). IPCE measurements were carried out using a Xenon lamp attached to a monochromator. Two focusing lenses were used to focus the monochromatic light to the active area of the solar cells. The device based on the standard hole-transporting material, spiro-OMeTAD, with both TBP and Li-TFSi showed the photovoltaic parameters: J_{sc} = 20.64 mA/cm^2; V_{oc} = 0.97 V; fill factor (FF) = 0.52; photoconversion efficiency (PCE) = 10.36% (Supplementary Fig. S9).

Results and discussion

Synthesis of hole-transporting polymers

The synthesis of **3,6-Cbz-EDOT** by DArP[47] and Stille polycondensation[48] was previously reported. Although the Stille polycondensation produced this polymer with the number-average molecular weight (M_n) of 2000 g/mol, DArP improved the M_n to 5600 g/mol (Scheme 1 and Table I). This result highlights the high potential of DArP for the synthesis of hole-transporting conjugated polymers.

In order to expand the applicability of DArP, the DTDPP monomer (**1**) was also polymerized under DArP conditions (Scheme 1). Since the DPP unit is a strong acceptor, electron-donating comonomer structures, such as triphenylamine (**2**) and fluorene (**3**), were selected to improve the intramolecular CT character. Thus, **DPP-OMe** and **DPP-F** were newly synthesized according to Scheme 1. First, the synthesis of **DPP-OMe** was evaluated from **1** and **2** under various DArP conditions (Table I). Under normal heating conditions, DArP did not provide the desired high molecular weight polymer regardless of the employed catalysts. The use of Herrmann's catalyst/P(*o*-OMePh)$_3$[49] afforded **DPP-OMe** with the M_n of 1700 g/mol, while the $Pd(OAc)_2/PCy_3HBF_4$ catalysts[50] slightly improved the M_n to 4700 g/mol. In order to further enhance the monomer reactivities, microwave heating conditions with 5 mol.% $Pd(OAc)_2$ as the catalyst and 1.5 equiv. of PivOK as the base in DMAc were adopted. It is well known that microwave heating efficiently increases the monomer reactivities and dramatically decreases the reaction time.[51] Although the heating to 100 °C for 1 h produced a negligible amount of the isolated polymer after Soxhlet extraction, a temperature increase to 120 °C resulted in the desired polymer with the M_n reaching 7900 g/mol in a reasonable yield (~60%). On the contrary, further prolongation or temperature increase lowered the M_n values. Consequently, the optimized microwave-assisted DArP conditions were determined to be 120 °C for 1 h. When these conditions were applied to the synthesis of **DPP-F**, a higher M_n of 12600 g/mol was achieved. This result suggested that the monomer structures of the aryl dibromides significantly affect the reactivity of DArP. It was postulated that the highly electron-rich triphenylamine unit lowers the oxidative addition efficiency of the Pd catalyst to the C–Br bonds.

https://doi.org/10.1557/mrc.2018.119 Published online by Cambridge University Press

Table I. Synthesis of hole-transporting conjugated polymers by direct arylation polycondensation.

Polymer	Conditions						Results	
	Catalyst	Ligand	Base	PivOH	Temp, time	Solvent	M_n (kg/mol)	M_w/M_n
DPP-OMe	$Pd(OAc)_2$ 5 mol.%	PCy_3HBF_4 10 mol.%	K_2CO_3 2.5 equiv.	PivOH 1 equiv.	120 °C, 24 h	DMAc/xylene, 1:1 mL	4.7	1.4
	Herrmann's catalyst 2 mol.%	P(*o*-OMePh)$_3$ 8 mol.%	Cs_2CO_3 2.3 equiv.	PivOH 20 mol.%	120 °C, 24 h	Toluene, 2 mL	1.7	1.7
	$Pd(OAc)_2$ 5 mol.%	–	PivOK 1.5 equiv.	–	100 °C, 1 h[a]	DMAc, 2 mL	[b]	[b]
	$Pd(OAc)_2$ 5 mol.%	–	PivOK 1.5 equiv.	–	120 °C, 1 h[a]	DMAc, 2 mL	**7.9**	**2.2**
	$Pd(OAc)_2$ 5 mol.%	–	PivOK 1.5 equiv.	–	120 °C, 3 h[a]	DMAc, 2 mL	7.0	1.8
	$Pd(OAc)_2$ 5 mol.%	–	PivOK 1.5 equiv.	–	140 °C, 1 h[a]	DMAc, 2 mL	6.6	1.8
DPP-F	$Pd(OAc)_2$ 5 mol.%	–	PivOK 1.5 equiv.	–	120 °C, 1 h[a]	DMAc, 2 mL	12.6	2.6
3,6-Cbz-EDOT[c]	$Pd(OAc)_2$ 5 mol.%	–	PivOK 1.5 equiv.	–	80 °C, 30 min[a]	DMAc, 2 mL	**5.6**	**1.9**

[a]Microwave heating.
[b]Nothing left after washing with hexane.
[c]Reported in Ref. 48.

The chemical structures of **DPP-OMe** and **DPP-F** were confirmed by their ^{1}H NMR spectra (Supplementary Fig. S1). The thermal properties of **DPP-OMe** and **DPP-F** were measured by TGA and DSC. The TGA showed that the 5% weight loss temperature ($T_{d5\%}$) of **DPP-OMe** and **DPP-F** was 267 and 378 °C, respectively (Supplementary Fig. S2). The DSC curves of both polymers did not reveal clear melting and crystallization peaks, but they exhibited a weak endothermic transition at 105 °C upon heating and an exothermic one at around 101–103 °C upon cooling, attributable to a glass transition for both polymers (Supplementary Fig. S3). All three polymers in this study were readily dissolved in common organic solvents, such as dichloromethane, chloroform and tetrahydrofuran. Thus, these polymers could be applied to HTMs in PSCs by using the convenient wet processes.

Optical and electrochemical properties

The UV-Vis absorption spectra of the polymers were measured in CH_2Cl_2 or in thin films (Supplementary Fig. S4). The absorption maximum of **3,6-Cbz-EDOT** was 354 nm in a solution and 374 nm in a thin film. The red shift of 20 nm from the solution to the film was due to the aggregation of the polymer chains in the solid state. The optical bandgap of **3,6-Cbz-EDOT**, calculated from the onset absorption of the thin film, was 2.75 eV (Table II). On the other hand, both **DPP-OMe** and **DPP-F** exhibited a longer wavelength absorption in the range of 500–700 nm due to the intramolecular CT. Accordingly, these polymers displayed narrow optical bandgaps of ~1.7 eV (Table II).

Cyclic voltammetry of the polymer films was measured in CH_3CN with 0.1 M $(n\text{-}C_4H_9)_4NPF_6$ as the supporting electrolyte. The HOMO and LUMO levels were calculated from the onset oxidation (E_{ox}) and onset reduction (E_{red}) potentials, respectively, under the assumption that Fc/Fc^+ locates at 4.80 eV below the vacuum level. **3,6-Cbz-EDOT** showed the E_{ox} of 0.16 V (versus Ag/Ag^+), which corresponds to the HOMO level of −4.87 eV (Supplementary Fig. S5). Due to the combination of the electron-donating monomers, no reduction peaks were observed in the measurement range. Therefore, the LUMO level (−2.12 eV) was estimated from the HOMO level and optical bandgap. In contrast, **DPP-OMe** and **DPP-F** displayed irreversible oxidation and reversible reduction peaks with the E_{ox} of around 0.39–0.60 V and E_{red} of −1.1 V. Both polymers possessed similar LUMO levels of −3.6 eV, probably because the DPP moiety has the dominant effect in determining the LUMOs. The HOMO levels were, on the contrary, determined by the triphenylamine and fluorene units, respectively. The determined HOMO levels were shallower than the valence band of $CH_3NH_3PbI_3$ (−5.45 eV), indicating that all three polymers are good HTM candidates for PSCs.

Hole mobilities

The hole mobilities of the HTMs are an important parameter to determine the efficiencies of the HTMs as well as the

https://doi.org/10.1557/mrc.2018.119 Published online by Cambridge University Press

Table II. Optical and electrochemical properties of the polymers.

	E_{ox} (V)[a]	E_{red} (V)[a]	HOMO (eV)	LUMO (eV)	Bandgap^{ec} (V)	Bandgap^{opt} (eV)
3,6-Cbz-EDOT	0.16	–	−4.87	−2.12	–	2.75
DPP-OMe	0.39	−1.12	−5.10	−3.59	1.51	1.68
DPP-F	0.60	−1.13	−5.31	−3.58	1.73	1.74

[a]Potentials versus Ag/Ag^+. $Fc/Fc^+ = 0.09$ V versus Ag/Ag^+.

performances of the PSCs. In order to estimate the hole mobilities of **3,6-Cbz-EDOT** and the DPP-based polymers, **DPP-OMe** and **DPP-F**, synthesized by DArP, top-contact/bottom-gate FET devices and hole-only devices were fabricated. In both fabrication processes, polymer solutions were prepared without the addition of any dopants, and the devices were measured in air without additional thermal or solvent annealing treatments. All the polymers exhibited a *p*-type charge transport behavior. Interestingly, it was reported that the hole mobility (μ) of **3,6-Cbz-EDOT**, synthesized by the Stille polycondensation, was 3.5×10^{-7} $cm^2/V/s$ in the FET.[48] However, the μ value increased to 1.48×10^{-5} $cm^2/V/s$ when the polymer was synthesized by DArP (Table III and Supplementary Fig. S6a). This result suggested that the polymer synthesized by the Stille polycondensation contains impurities and DArP is a better method of producing high mobility polymers. Although we did not prepare the control samples of the **DPP-OMe** and **DPP-F** by the Stille polycondensation, they may show similar behaviors. The FET mobilities of **DPP-OMe** and **DPP-F** were 2.93×10^{-5} and 4.45×10^{-4} $cm^2/V/s$, respectively (Table III and Supplementary Fig. S6a).

The FET mobilities mainly reflect the charge transport in the in-plane direction.[52–54] However, photovoltaic devices require high mobilities in the out-of-plane direction. Therefore, in order to evaluate the out-of-plane mobilities of the polymer films, hole-only devices were fabricated by the simple spin-coating technique, and the mobilities were determined by a SCLC method (Supplementary Fig. S6b). As a result, the μ value of **3,6-Cbz-EDOT**, synthesized by DArP in this study, was 2.69×10^{-5} $cm^2/V/s$, which was almost two times higher than the FET mobility (Table II). In contrast, the μ values of **DPP-OMe** (1.02×10^{-6} cm^2/V) and **DPP-F** (1.76×10^{-5} cm^2/V) decreased by one order of magnitude as compared with those determined by FET. These results suggested that **3,6-Cbz-EDOT** predominantly forms a face-on orientation, while **DPP-OMe** and **DPP-F** prefer an edge-on orientation in their thin films. As already described, photovoltaic devices including PSCs require fast carrier transport in the direction perpendicular to the film plane (out-of-plane). Thus, it was postulated that the SCLC mobilities are more strongly associated with the photovoltaic properties and **3,6-Cbz-EDOT** is a more promising HTM than the other two polymers.

Surface hydrophobicity and PSC fabrication

In the PSCs, the perovskite layer is very sensitive to water.[55] Therefore, one of the main roles of the HTMs is to protect the perovskite nanoparticles from water in the air. The hydrophobic nature of hole-transporting conjugated polymers is thus significant. Also, in order to enhance the photovoltaic performances, some dopants, such as the Li-TFSi[56] and TBP,[57] are often added to the hole-transport layer of the PSCs. It is said that Li-TFSi increases the electrical conductivity of the hole-transport layer, while TBP promotes the formation of homogeneous films.[58] It is noteworthy that the hydrophobicity changes in the hole-transport layer after the addition of these dopants. The water contact angles of the polymer thin films were measured, and the results are shown in Supplementary Fig. S7. The pristine polymer films without any dopants exhibited highly hydrophobic properties with the contact angles above 90°, e.g., 92.7° for **3,6-Cbz-EDOT** (Supplementary Figs. S7a–S7c). However, when TBP (92 wt.% relative to the polymer) was added to **3,6-Cbz-EDOT**, the contact angle slightly decreased to 84.7° (Supplementary Fig. S7d). The addition of Li-TFSi (5.7 wt.% relative to the polymer) resulted in a dramatic decrease in the contact angle to 30.9°

Table III. Performances of field-effect transistor (FET) devices and hole-only devices.

HTM	FET hole mobility ($cm^2/V/s$)	I_{on}/I_{off}	SCLC hole mobility ($cm^2/V/s$)	Film thickness (nm)	Slope of SCLC regime in log–log plot
3,6-Cbz-EDOT	1.48×10^{-5}	10^2–10^3	2.69×10^{-5}	75	1.96
DPP-OMe	2.93×10^{-5}	10^2–10^3	1.02×10^{-6}	72	2.03
DPP-F	4.45×10^{-4}	10^3–10^4	1.76×10^{-5}	70	2.03

https://doi.org/10.1557/mrc.2018.119 Published online by Cambridge University Press

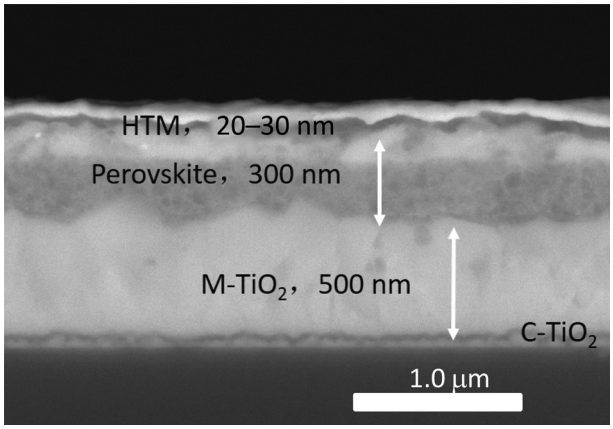


Figure 1. A cross-sectional SEM micrograph of the PSC based on **3,6-Cbz-EDOT**.

(Supplementary Fig. S7e). Finally, when both dopants were added, the contact angle eventually became 28.5° (Supplementary Fig. S7f). However, a sufficient electrical conductivity of the hole-transport layer is achieved at the cost of the hydrophobicity. This trade-off relationship is clearly seen in the device stability study (vide infra).

Based on the optical and electrochemical properties, the HOMO and LUMO energy levels of the three polymers were determined and summarized in Table II (vide supra). For the efficient carrier transport, the HTMs should possess HOMO levels slightly shallower (no more than 0.5 eV) than the valence band of the perovskite ($CH_3NH_3PbI_3$) layers. In this sense, the HOMO levels of all three polymers in this study were suitable as HTMs in the PSCs. Compared with the DPP-based polymers, **3,6-Cbz-EDOT** exhibited a shallower LUMO level, indicating its better electron blocking property.[59] PSCs based on these polymers were fabricated with the FTO/compact-TiO_2/mesoporous-TiO_2/HTM/Au configuration. Each layer of the PSCs was confirmed by the cross-sectional view from a SEM analysis (Fig. 1). The devices consisted of a 500 nm-thick mesoporous TiO_2 (M-TiO_2) layer and 300 nm-thick perovskite layer. Since the perovskite nanoparticles grew on the surface of the M-TiO_2, there was an overlap of these two layers. However, due to the good film forming ability, the thickness of the hole-transport layer was only 20–30 nm. On the top, an 80 nm-thick Au contact was deposited by vacuum evaporation.

Photovoltaic performances

We measured the current J–V characteristics of the PSCs based on the developed HTMs under illumination of a solar simulator with the light intensity of 100 mW/cm^2 (AM 1.5). First, the devices based on the HTMs without any dopants were compared. It was previously reported that the device based on **3,6-Cbz-EDOT**, synthesized by the Stille polycondensation, showed the PCE of 3.90%.[48] With the same device structure and measurement conditions, **3,6-Cbz-EDOT**, synthesized by DArP, improved the PCE to 4.30% (Table IV and Supplementary Fig. S8a). This result was consistent with that of the FET mobilities (vide supra). It should be highlighted again that DArP produces highly pure conjugated polymers. The devices based on **DPP-OMe** and **DPP-F** displayed similar PCEs of 3.42–4.00%. However, there was a noticeable difference in the J_{sc} values, which are related to the carrier mobilities. The order of the short-circuit current density (J_{sc}) was **3,6-Cbz-EDOT** > **DPP-F** > **DPP-OMe** (Table IV). This order was consistent with that of the SCLC mobilities (vide supra) as well as the IPCE spectra (Supplementary Fig. S8b). This result supports the idea that the SCLC mobilities are more strongly associated with the photovoltaic properties of the PSCs than the FET mobilities.

Table IV. Summary of the PSC performances (FTO/compact-TiO_2/mesoporous-TiO_2/HTM/Au).

HTM	Dopant	J_{sc} (mA/cm^2)	V_{oc} (V)	FF	PCE (%)
3,6-Cbz-EDOT	Undoped	15.40	0.82	0.34	4.30
	TBP	15.65	0.93	0.47	6.85
	Li-TFSi	17.47	0.94	0.38	6.39
	TBP + Li-TFSi	17.81	0.92	0.50	8.13
3,6-Cbz-EDOT[a]	Undoped	14.70	0.80	0.32	3.90
DPP-OMe	Undoped	11.69	0.83	0.41	4.00
	TBP + Li-TFSi	11.07	0.78	0.47	4.06
DPP-F	Undoped	13.30	0.77	0.33	3.42
	TBP + Li-TFSi	13.29	0.77	0.39	3.97

[a]Synthesized by Stille coupling polycondensation reported in Ref. 48.

https://doi.org/10.1557/mrc.2018.119 Published online by Cambridge University Press

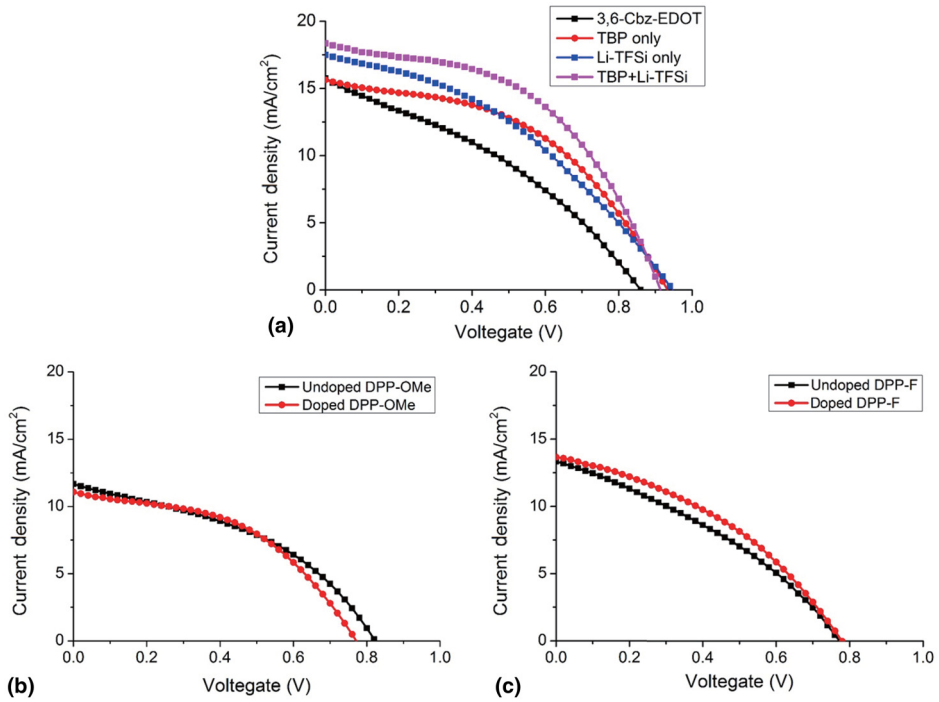


Figure 2. Current–voltage (J–V) curves of the PSCs based on (a) **3,6-Cbz-EDOT**, (b) **DPP-OMe**, and (c) **DPP-F** with or without dopants.

In order to optimize the photovoltaic performances, the dopants (Li-TFSi and TBP) were added to the spin-coating solution of the HTMs. The effects of the added dopants were different depending on the polymers. For example, **3,6-Cbz-EDOT**, synthesized by DArP, had significant positive effects. When TBP was added, the PCE increased to 6.85% mainly due to the increase in the FF [Table IV and Fig. 2(a)]. In addition to the homogeneous film formation, TBP controls the interface between the HTMs and perovskite layer.[56] Thus, the observed increase in FF was ascribed to the well-defined interface production. The addition of Li-TFSi also resulted in a positive effect. As compared with the device without any additives, a higher J_{sc} ($15.40 \rightarrow 17.47$ mA/cm^2) and improved PCE (6.39%) were produced [Table IV and Fig. 2(a)]. This was probably due to the higher mobility of the hole-transport layer, realized by the efficient doping (the possibility of oxygen doping was also suggested[60]). Adding both dopants resulted in a positive synergistic effect. Thus, both J_{sc} and FF retained higher values, leading to the best PCE of 8.13%.

The dopant effects were also studied for the devices based on **DPP-OMe** and **DPP-F**. Although slight increases in the PCEs were observed by the addition of TBP and Li-TFSi, they were not significant [Table IV and Figs. 2(b) and 2(c)]. This may have been caused by the difficult doping due to the

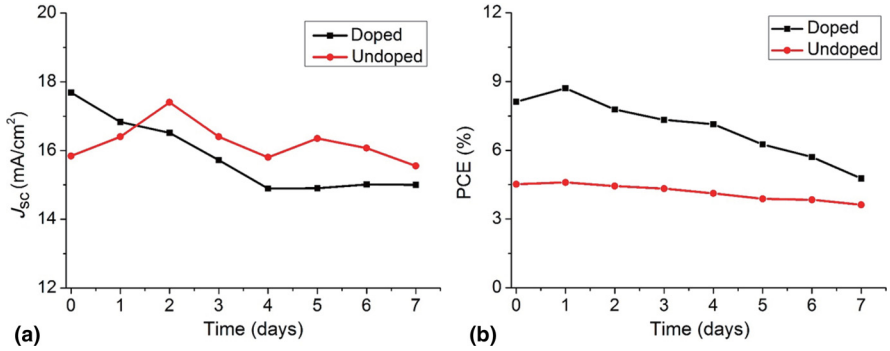


Figure 3. Time-dependent decay of the photovoltaic parameters, (a) J_{sc} and (b) PCE, of the device based on **3,6-Cbz-EDOT**.

https://doi.org/10.1557/mrc.2018.119 Published online by Cambridge University Press

deep HOMOs of these polymers. Also, the predominant polymer orientation (edge-on) might have cancelled the positive doping effect in the PSCs.

Device stability

The air stability of the PSCs was evaluated by time-dependent measurements of the devices based on the doped (both Li-TFSi and TBP) or undoped (pristine) **3,6-Cbz-EDOT**. All the devices were stored in the dark in air. The changes in the J_{sc} and PCE for 1 week are shown in Fig. 3. The results suggested that both the J_{sc} and PCE of the device based on the doped **3,6-Cbz-EDOT** gradually decreased by 15% after 1 week. As already described, the addition of Li-TFSi to the hole-transport layer enhanced the hole mobility, but at the same time, lowered the hydrophobicity. The latter effect caused degradation of the perovskite layer and related interfaces. On the other hand, when no dopants were added, both J_{sc} and PCE were lower but they were more stable. Overall, the decrease in the photovoltaic parameters of the device based on the undoped **3,6-Cbz-EDOT** was negligible even after 1 week.

Conclusion

In summary, we demonstrated that microwave-assisted DArP is a powerful method of synthesizing hole-transporting conjugated polymers in a short reaction time. The polymer synthesized by DArP exhibited a higher hole mobility and photovoltaic performances in the PSCs than that synthesized by the conventional Stille polycondensation. It was also shown that the chemical doping of the hole-transport layer of the PSCs with Li-TFSi and TBP is not always effective. The face-on dominant polymer, revealed by the two types of mobility measurements, namely, FET and SCLC, improved the photovoltaic properties by doping. However, the edge-on dominant polymers did not display well-defined positive doping effects. All these findings are useful for the future design of new high-performance hole-transporting conjugated polymers.

Supplementary material

The supplementary material for this article can be found at https://doi.org/10.1557/mrc.2018.119.

Acknowledgments

This work was supported by the Heiwa Nakajima Foundation, the Ogasawara Foundation for the Promotion of Science and Technology, the Yazaki Memorial Foundation for Science and Technology, the SEI Group CRS Foundation, and the Support for Tokyotech Advanced Researcher.

References

1. Y. Shirota and H. Kageyama: Charge carrier transporting molecular materials and their applications in devices. *Chem. Rev.* **107**, 953 (2007).
2. J. Wang, K. Liu, L. Ma, and X. Zhan: Triarylamine: versatile platform for organic, dye-sensitized, and perovskite solar cells. *Chem. Rev.* **116**, 14675 (2016).
3. L. Calió, S. Kazim, M. Grätzel, and S. Ahmad: Hole-transporting materials for perovskite solar cells. *Angew. Chem. Int. Ed.* **55**, 14522 (2016).
4. S. Ameen, M.A. Rub, S.A. Kosa, K.A. Alamry, M.S. Akhtar, H.-S. Shin, H.-K. Seo, A.M. Asiri, and M.K. Nazeeruddin: Perovskite solar cells: influence of hole transporting materials on power conversion efficiency. *ChemSusChem.* **9**, 10 (2016).
5. P. Agarwala and D. Kabra: A review on triphenylamine (TPA) based organic hole transport materials (HTMs) for dye sensitized solar cells (DSSCs) and perovskite solar cells (PSCs): evolution and molecular engineering. *J. Mater. Chem. A* **5**, 1348 (2017).
6. A. Krishna and A.C. Grimsdale: Hole transporting materials for mesoscopic perovskite solar cells—towards a rational design? *J. Mater. Chem. A* **5**, 16446 (2017).
7. C. Rodríguez-Seco, L. Cabau, A. Vidal-Ferran, and E. Palomares: Advances in the synthesis of small molecules as hole transport materials for lead halide perovskite solar cells. *Acc. Chem. Res.* **51**, 869 (2018).
8. W. Zhou, Z. Wen, and P. Gao: Less is more: dopant-free hole transporting materials for high-efficiency perovskite solar cells. *Adv. Energy Mater.* **8**, 1702512 (2018).
9. Y. Tao, C. Yang, and J. Qin: Organic host materials for phosphorescent organic light-emitting diodes. *Chem. Soc. Rev.* **40**, 2943 (2011).
10. J. Veres, S.D. Ogier, S.W. Leeming, D.C. Cupertino, and S.M. Khaffaf: Low-k insulators as the choice of dielectrics in organic field-effect transistors. *Adv. Funct. Mater.* **13**, 199 (2003).
11. M. Horie, Y. Luo, J.J. Morrison, L.Z. Majewski, A. Song, B.R. Saunders, and M.L. Turner: Triarylamine polymers by microwave-assisted polycondensation for use in organic field-effect transistors. *J. Mater. Chem.* **18**, 5230 (2008).
12. T. Michinobu, H. Kumazawa, E. Otsuki, H. Usui, and K. Shigehara: Synthesis and properties of nitrogen-linked poly(2,7-carbazole)s as hole-transport material for organic light emitting materials. *J. Polym. Sci. Part A* **47**, 3880 (2009).
13. K. Tsuchiya, T. Shimomura, and K. Ogino: Preparation of diblock copolymer based on poly(4-*n*-butyltriphenylamine) via palladium coupling polymerization. *Polymer* **50**, 95 (2009).
14. K. Tsuchiya, T. Sakakura, and K. Ogino: Synthesis of triphenylamine copolymers and effect of their chemical structures on physical properties. *Macromolecules* **44**, 5200 (2011).
15. L.-T. Huang, H.-J. Yen, and G.-S. Liou: Substituent effect on electrochemical and electrochromic behaviors of ambipolar aromatic polyimides based on aniline derivatives. *Macromolecules* **44**, 9595 (2011).
16. A. Iwan and D. Sek: Polymers with triphenylamine units: photonic and electroactive materials. *Prog. Polym. Sci.* **36**, 1277 (2011).
17. Y.-G. Ko, W. Kwon, H.-J. Yen, C.-W. Chang, D.M. Kim, K. Kim, S. G. Hahm, T.J. Lee, G.-S. Liou, and M. Ree: Various digital memory behaviors of functional aromatic polyimides based on electron donor and acceptor substituted triphenylamines. *Macromolecules* **45**, 3749 (2012).
18. T. Michinobu, C. Seo, K. Noguchi, and T. Mori: Effects of click postfunctionalization on thermal stability and field effect transistor performances of aromatic polyamines. *Polym. Chem.* **3**, 1427 (2012).
19. C.-J. Chen, Y.-C. Hu, and G.-S. Liou: Linkage and acceptor effects on diverse memory behavior of triphenylamine-based aromatic polymers. *Polym. Chem.* **4**, 4162 (2013).
20. O. Malinkiewicz, A. Yella, Y.H. Lee, G.M. Espallargas, M. Graetzel, M. K. Nazeeruddin, and H.J. Bolink: Perovskite solar cells employing organic charge-transport layers. *Nat. Photon.* **8**, 128 (2014).
21. H.-J. Yen, J.-H. Lin, Y.O. Su, and G.-S. Liou: Novel triarylamine-based aromatic polyamides bearing secondary amines: synthesis and redox potential inversion characteristics induced by pyridines. *J. Mater. Chem. C* **4**, 10381 (2016).
22. K. Suwa, S. Tanaka, K. Oyaizu, and H. Nishide: Arylamine polymers prepared via facile paraldehyde addition condensation: an effective hole-transporting materials for perovskite solar cells. *Polym. Int.* **67**, 670 (2018).
23. L. Bian, E. Zhu, J. Tang, W. Tang, and F. Zhang: Recent progress in the design of narrow bandgap conjugated polymers for high-efficiency organic solar cells. *Prog. Polym. Sci.* **37**, 1292 (2012).
24. C. Liu, K. Wang, X. Gong, and A.J. Heeger: Low bandgap semiconducting polymers for polymeric photovoltaics. *Chem. Soc. Rev.* **45**, 4825 (2016).
25. Y. Wang and T. Michinobu: Benzothiadiazole and its π-extended, heteroannulated derivatives: useful acceptor building blocks for high-performance donor-acceptor polymers in organic electronics. *J. Mater. Chem. C* **4**, 6200 (2016).

https://doi.org/10.1557/mrc.2018.119 Published online by Cambridge University Press

26. L. Ying, F. Huang, and G.C. Bazan: Regioregular narrow-bandgap-conjugated polymers for plastic electronics. *Nat. Commun.* **8**, 14047 (2017).
27. Y. Li, M. Gu, Z. Pan, B. Zhang, X. Yang, J. Gu, and Y. Chen: Indacenodithiophene: a promising building block for high performance polymer solar cells. *J. Mater. Chem. A* **5**, 10798 (2017).
28. P. Sonar, S.P. Singh, Y. Li, M.S. Soh, and A. Dodabalapur: A low-bandgap diketopyrrolopyrrole-benzothiadiazole-based copolymer for high-mobility ambipolar organic thin-film transistors. *Adv. Mater.* **22**, 5409 (2010).
29. Z. Yi, S. Wang, and Y. Liu: Design of high-mobility diketopyrrolopyrrole-based π-conjugated copolymers for organic thin-film transistors. *Adv. Mater.* **27**, 3589 (2015).
30. W. Li, K.H. Hendriks, M.M. Wienk, and R.A.J. Janssen: Diketopyrrolopyrrole polymers for organic solar cells. *Acc. Chem. Res.* **49**, 78 (2016).
31. A. Facchetti, L. Vaccaro, and A. Marrochi: Semiconducting polymers prepared by direct arylation polycondensation. *Angew. Chem. Int. Ed.* **51**, 3520 (2012).
32. L.G. Mercier and M. Leclerc: Direct (hetero)arylation: a new tool for polymer chemists. *Acc. Chem. Res.* **46**, 1597 (2013).
33. S. Kowalski, S. Allard, K. Zilberberg, T. Riedl, and U. Scherf: Direct arylation polycondensation as simplified alternative for the synthesis of conjugated (co)polymers. *Prog. Polym. Sci.* **38**, 1805 (2013).
34. A.E. Rudenko and B.C. Thompson: Optimization of direct arylation polymerization (DArP) through the identification and control of defects in polymer structure. *J. Polym. Sci. Part A* **53**, 135 (2015).
35. J.-R. Pouliot, F. Grenier, J.T. Blaskovits, S. Beaupré, and M. Leclerc: Direct (hetero)arylation polymerization: simplicity for conjugated polymer synthesis. *Chem. Rev.* **116**, 14225 (2016).
36. T. Bura, J.T. Blaskovits, and M. Leclerc: Direct (hetero)arylation polymerization: trends and perspectives. *J. Am. Chem. Soc.* **138**, 10056 (2016).
37. S.-L. Suraru, J.A. Lee, and C.K. Luscombe: C-H arylation in the synthesis of π-conjugated polymers. *ACS Macro Lett.* **5**, 724 (2016).
38. H. Bohra and M. Wang: Direct C-H arylation; a "greener" approach towards facile synthesis of organic semiconducting molecules and polymers. *J. Mater. Chem. A* **5**, 11550 (2017).
39. S. Yu, F. Liu, J. Yu, S. Zhang, C. Cabanetos, Y. Gao, and W. Huang: Eco-friendly direct (hetero)-arylation polymerization: scope and limitation. *J. Mater. Chem. C* **5**, 29 (2017).
40. P. Berrouard, A. Najari, A. Pron, D. Gendron, P.-O. Morin, J.-R. Pouliot, J. Veilleux, and M. Leclerc: Synthesis of 5-alkyl[3,4-*c*] thienopyrrole-4,6-dione-based polymers by direct heteroarylation. *Angew. Chem. Int. Ed.* **51**, 2068 (2012).
41. S.-W. Chang, H. Waters, J. Kettle, Z.-R. Kuo, C.-H. Li, C.-Y. Yu, and M. Horie: Pd-catalysed direct arylation polymerisation for synthesis of low-bandgap conjugated polymers and photovoltaic performance. *Macromol. Rapid Commun.* **33**, 1927 (2012).
42. Y. Gao, X. Zhang, H. Tian, J. Zhang, D. Yang, Y. Geng, and F. Wang: High mobility ambipolar diketopyrrolopyrrole-based conjugated polymer synthesized via direct arylation polycondensation. *Adv. Mater.* **27**, 6753 (2015).
43. H. Song, Y. Deng, Y. Gao, Y. Jiang, H. Tian, D. Yan, Y. Gen, and F. Wang: Donor-acceptor conjugated polymers based on indacenodithiophene derivative bridged diketopyrrolopyrroles: synthesis and semiconducting properties. *Macromolecules* **50**, 2344 (2017).
44. H. Saito, J. Chen, J. Kuwabara, T. Yasuda, and T. Kanbara: Facile one-pot access to π-conjugated polymers *via* sequential bromination/direct arylation polycondensation. *Polym. Chem.* **8**, 3006 (2017).
45. Y. Li, W.J.K. Tatum, J.W. Onorato, S.D. Barajas, Y.Y. Yang, and C. K. Luscombe: An indacenodithiophene-based semiconducting polymer with high ductility for stretchable organic electronics. *Polym. Chem.* **8**, 5185 (2017).
46. J. Kuwabara, T. Yasuda, S.J. Choi, W. Lu, K. Yamazaki, S. Kagaya, L. Han, and T. Kanbara: Direct arylation polycondensation: a promising method for the synthesis of highly pure, high-molecular-weight conjugated polymers needed for improving the performance of organic photovoltaics. *Adv. Funct. Mater.* **24**, 3226 (2014).
47. W. Li and T. Michinobu: Structural effects of dibromocarbazoles on direct arylation polycondensation with 3,4-ethylenedioxythiophene. *Polym. Chem.* **7**, 3165 (2016).
48. W. Li, M. Otsuka, T. Kato, Y. Wang, T. Mori, and T. Michinobu: 3,6-Carbazole vs 2,7-carbazole: a comparative study of hole-transporting polymeric materials for inorganic-organic hybrid perovskite solar cells. *Beilstein J. Org. Chem.* **12**, 1401 (2016).
49. J.-R. Pouliot, B. Sun, M. Leduc, A. Najari, Y. Li, and M. Leclerc: A high mobility DPP-based polymer obtained *via* direct (hetero)arylation polymerization. *Polym. Chem.* **6**, 278 (2015).
50. K. Wang, G. Wang, and M. Wang: Balanced ambipolar poly (diketopyrrolopyrrole-*alt*-tetrafluorobenzene) semiconducting polymers synthesized via direct arylation polymerization. *Macromol. Rapid Commun.* **36**, 2162 (2015).
51. M.B. Gawande, S.N. Shelke, R. Zboril, and R.S. Varma: Microwave-assisted chemistry: synthetic applications for rapid assembly of nanomaterials and organics. *Acc. Chem. Res.* **47**, 1338 (2014).
52. C.J. Mueller, E. Gann, C.R. Singh, M. Thelakkat, and C.R. McNeill: Role of the dopants on the morphological and transport properties of spiro-MeOTAD hole transport layer. *Chem. Mater.* **28**, 7088 (2016).
53. Y. Wang, T. Hasegawa, H. Matsumoto, T. Mori, and T. Michinobu: Rational design of high-mobility semicrystalline conjugated polymers with tunable charge polarity: beyond benzobisthiadiazole-based polymers. *Adv. Funct. Mater.* **27**, 1604608 (2017).
54. Y. Wang, T. Hasegawa, H. Matsumoto, T. Mori, and T. Michinobu: High-performance n-channel organic transistors using high-molecular-weight electron-deficient copolymers and amine-tailed self-assembled monolayers. *Adv. Mater.* **30**, 1707164 (2018).
55. I. Lee, J.H. Yun, H.J. Son, and T.-S. Kim: Accelerated degradation due to weakened adhesion from Li-TFSi additives in perovskite solar cells. *ACS Appl. Mater. Interfaces* **9**, 7029 (2017).
56. R. Schölin, M.H. Karlsson, S.K. Eriksson, H. Siegbahn, E.M.J. Johansson, and H. Rensmo: Energy level shifts in spiro-OMeTAD molecular thin films when adding Li-TFSI. *J. Phys. Chem. C* **116**, 26300 (2012).
57. S.N. Habisreutinger, N.K. Noel, H.J. Snaith, and R.J. Nicholas: Investigating the role of 4-*tert* butylpyridine in perovskite solar cells. *Adv. Energy Mater.* **7**, 1601079 (2017).
58. E.J. Juarez-Perez, M.R. Leyden, S. Wang, L.K. Ono, Z. Hawash, and Y. Qi: Role of the dopants on the morphological and transport properties of spiro-MeOTAD hole transport layer. *Chem. Mater.* **28**, 5702 (2018).
59. Y. Xiao, G. Han, J. Wu, and J.-Y. Lin: Efficient bifacial perovskite solar cell based on a highly transparent poly(3,4-ethylenedioxythiophene) as the p-type hole-transporting material. *J. Power Sources* **306**, 171 (2016).
60. A. Abate, T. Leijtens, S. Pathak, J. Teuscher, R. Avolio, M.E. Errico, J. Kirkpatrik, J.M. Ball, P. Docampo, I. McPherson, and H.J. Snaith: Lithium salts as "redox active" p-type dopants for organic semiconductors and their impact in solid-state dye-sensitized solar cells. *Phys. Chem. Chem. Phys.* **15**, 2572 (2013).

Table of contents

Hole-transporting conjugated polymers synthesized by direct arylation polycondensation show higher hole mobilities and better photovoltaic performances of the perovskite solar cells than those synthesized by the conventional Stille coupling polycondensation.

https://doi.org/10.1557/mrc.2018.119 Published online by Cambridge University Press